From REZnSn to REZnSnH1.5 (RE = Pr, Nd) - Inducing ferromagnetism through hydrogenation

Bastian Reker, Bernard Chevalier, Oliver Niehaus, Ute Ch. Rodewald, Rainer Pöttgen

From *RE*ZnSn to *RE*ZnSnH$_{1.5}$ (*RE* = Pr, Nd) – Inducing Ferromagnetism through Hydrogenation

Bastian Reker[a], Bernard Chevalier[b], Oliver Niehaus[a], Ute Ch. Rodewald[a], and Rainer Pöttgen[a]

[a] Institut für Anorganische und Analytische Chemie, Universität Münster, Corrensstrasse 30, 48149 Münster, Germany

[b] CNRS, Université de Bordeaux, ICMCB, 87 Avenue Dr. A. Schweitzer, F-33608 Pessac-Cedex, France

Reprint requests to R. Pöttgen. E-mail: pottgen@uni-muenster.de

Z. Naturforsch. **2013**, *68b*, 1191 – 1197 / DOI: 10.5560/ZNB.2013-3199
Received July 23, 2013

The ternary stannides PrZnSn and NdZnSn were synthesized by induction-melting of the elements in sealed tantalum tubes. They were characterized by powder and single-crystal X-ray diffraction: YPtAs-type structure, $P6_3/mmc$, $a = 455.4(1)$ and $c = 1650.3(2)$ pm, $wR2 = 0.0266$, 297 F^2 for PrZnSn and $a = 453.7(1)$ and $c = 1637.0(4)$ pm, $wR2 = 0.1558$, 234 F^2 for NdZnSn with 12 variables per refinement. PrZnSn and NdZnSn are AlB_2 superstructures with slightly puckered and ordered $[Zn_3Sn_3]$ hexagons in AA′BB′ stacking sequence along the crystallographic *c* axis. Hydrogenation results in the new hexagonal hydrides PrZnSnH$_{1.5}$ ($a = 447.98(8)$ and $c = 1707.5(5)$ pm) and NdZnSnH$_{1.5}$ ($a = 448.28(8)$ and $c = 1689.8(2)$ pm). Filling of RE_3Zn tetrahedra by hydrogen leads to anisotropic changes of the lattice parameters and a drastic flattening of the $[Zn_3Sn_3]$ layers. Temperature-dependent magnetic susceptibility measurements show Curie-Weiss behavior for PrZnSn and NdZnSn with experimental magnetic moments close to the free-ion values of RE^{3+}. Magnetic ordering is detected at 4.7 (PrZnSn) and 6.5 K (NdZnSn). Hydrogenation induces ferromagnetism with increased ordering temperatures of 12.0 (PrZnSnH$_{1.5}$) and 14.5 K (NdZnSnH$_{1.5}$).

Key words: Stannides, Hydrogenation, Magnetic Properties

Introduction

The equiatomic rare earth (*RE*) transition metal (*T*) stannides *RET*Sn have intensively been studied with respect to their crystal chemistry as well as their magnetic and electrical properties [1]. Most of the *RET*Sn stannides crystallize with superstructures of the aristotype AlB_2 [2 – 4], with the hexagonal ZrNiAl [5 – 7] or the cubic MgAgAs (so-called Half-Heusler phase) type [8, 9]. Only CeRuSn [10, 11] forms its own peculiar structure type which is a consequence of strong covalent Ce–Ru bonding associated with almost tetravalent cerium.

Modification of the magnetic ground states of the *RET*Sn stannides is possible through (i) solid solutions, *e. g.* Ce(Ni$_{1-x}$Rh$_x$)Sn [12] or Ce(Ni$_{1-x}$Cu$_x$)Sn [13], (ii) *via* high-pressure high-temperature treatment, *e. g.* Ce*T*Sn (*T* = Ni, Pd, Pt) [14 – 16], or (iii) through hydrogenation reactions [17 – 22]. Striking examples for the hydrogenation reactions are the Kondo insulator CeNiSn which transforms to the 7 K ferromagnet CeNiSnH$_{1.8}$ [17] and leads to an increase of the Curie temperature from 4.8 (CeZnSn) to 7.3 K (CeZnSnH$_{1.5}$) [22].

In continuation of our systematic studies of hydrogenation-induced property changes of *RET*Sn ternary stannides and related equiatomic compounds we have performed hydrogenation reactions on PrZnSn and NdZnSn which are isotypic with CeZnSn [23]. So far, both stannides have only been characterized on the basis of powder X-ray diffraction data [24 – 26]. Herein we report on single-crystal data, the magnetic behavior of PrZnSn and NdZnSn and their hydrogenation reactions to PrZnSnH$_{1.5}$ and NdZnSnH$_{1.5}$ which strongly change their magnetic ground state.

Experimental

Synthesis and hydrogenation

Starting materials for the syntheses of the ternary stannides PrZnSn and NdZnSn were sublimed pieces of praseodymium and neodymium (smart elements, > 99.9 %), and zinc and tin granules (Merck, > 99.9 %). Pieces of the elements were weighed in the ideal atomic 1 : 1 : 1 ratio and arc-welded [27] in small tantalum ampoules under an argon atmosphere of *ca*. 700 mbar. The argon was purified over titanium sponge (900 K), silica gel, and molecular sieves. The tubes were placed in a water-cooled quartz sample chamber of an induction furnace (Hüttinger Elektronik, Freiburg, type TIG 1.5/300) [28] and first rapidly heated to *ca*. 1450 K and kept at that temperature for 15 min. The temperature was then lowered to 800 K, and the tubes were annealed for another five hours. Finally the samples were cooled to r. t. by switching off the power supply. The temperature was controlled through a Sensor Therm Methis MS09 pyrometer with an accuracy of ±30 K. Both samples could easily be separated from the tantalum tube by mechanical fragmentation. They are air-stable over weeks. The powdered samples are dark gray, and single crystals exhibit metallic luster.

Hydrogen absorption experiments were performed using the apparatus reported previously for the hydrogenation of CeZnSn [22]. Small pieces of the annealed PrZnSn and NdZnSn samples were heated under vacuum at 553 K for 4 h and then exposed to 4 MPa of hydrogen gas (99.999 % as purity) at the same temperature for two days. The hydrogenation induces a decrepitation of the starting stannides. The amount of hydrogen absorbed was determined volumetrically by monitoring pressure changes in a calibrated volume. Under these conditions, the new hydrides PrZnSnH$_{1.5}$ and NdZnSnH$_{1.5}$ were obtained. They are stable under ambient conditions.

EDX data

Semiquantitative EDX analyses of the single crystals studied on the diffractometer were carried out in variable pressure mode with a Zeiss EVO® MA10 scanning electron microscope with PrF_3, NdF_3, Zn, and Sn as standards. The experimentally observed average compositions were close to the ideal ones. The irregular surface of the crystals (conchoidal fracture) hampered the determination of precise compositions. No impurity elements (especially from the container material) were detected.

X-Ray diffraction

The polycrystalline samples of PrZnSn and NdZnSn and their hydrides were characterized by powder X-ray diffraction using the Guinier technique: imaging plate detector, Fujifilm BAS-1800, Cu$K_{\alpha 1}$ radiation and α-quartz ($a = 491.30$ and $c = 540.46$ pm) as an internal standard. The hexagonal lattice parameters (Table 1) were calculated from the Guinier powder data by standard least-squares refinements. The experimental patterns were compared to calculated ones [29] in order to assure correct indexing. Our data show reasonable agreement with earlier results (Table 1).

Table 1. Lattice parameters (Guinier powder data) of the hexagonal ternary stannides *RE*ZnSn (*RE* = Ce, Pr, Nd) and their hydrides *RE*ZnSnH$_{1.5}$. Standard deviations are given in parentheses.

Compound	*a* (pm)	*c* (pm)	*V* (nm^3)	Reference
CeZnSn	456.5(1)	1670.8(2)	0.3015	[26]
CeZnSn	456.7(3)	1673.8(5)	0.3023	[23]
CeZnSnH$_{1.5}$	449.34(9)	1731.3(4)	0.3027	[22]
PrZnSn	455.4(1)	1653.7(2)	0.2970	[26]
PrZnSn	455.4(1)	1650.3(2)	0.2964	this work
PrZnSnH$_{1.5}$	447.98(8)	1707.5(5)	0.2967	this work
NdZnSn	453.2(1)	818.3(3)	0.1456	[24]
NdZnSn	454.81(9)	748.4(2)	0.1341	[25]
NdZnSn	454.3(1)	1638.8(2)	0.2929	[26]
NdZnSn	453.7(1)	1637.0(4)	0.2918	this work
NdZnSnH$_{1.5}$	448.28(8)	1689.8(2)	0.2941	this work

Single crystals of PrZnSn and NdZnSn were selected from the crushed annealed samples, glued to quartz fibers using beeswax and characterized on a Buerger camera (using white Mo radiation) to check their quality. Intensity data of the PrZnSn crystal were collected at room temperature by use of a four-circle diffractometer (Enraf-Nonius CAD4) with graphite-monochromatized MoK_α radiation (71.073 pm) and a scintillation counter with pulse height discrimination. The scans were performed in the $\omega/2\theta$ mode. The NdZnSn crystal was measured on a Stoe IPDS-II image plate system (graphite-monochromatized MoK_α radiation; λ = 71.073 pm) in oscillation mode. Numerical absorption corrections were applied to the data sets. Details of the data collections and the crystallographic parameters are summarized in Table 2.

Structure refinements

Isotypism of PrZnSn and NdZnSn with CeZnSn [23] was evident from the Guinier powder data which already showed the weak superstructure reflections forcing the quadrupled *c* axis. The systematic extinctions of the data sets were compatible with space group $P6_3/mmc$. The atomic parameters of CeZnSn were taken as starting values, and both structures were refined with anisotropic displacement parameters for all atoms with SHELXL-97 (full-matrix least-squares on F_o^2) [30, 31]. As a check for the correct composition, the occupancy parameters were refined in separate series of least-squares cycles for both data sets. All sites were fully occupied within two standard deviations, and the ideal compo-

Table 2. Crystal data and structure refinement results for the ternary stannides PrZnSn and NdZnSn, YPtAs type, $P6_3/mmc$, $Z = 2$.

Compound	PrZnSn	NdZnSn
Molar mass, g mol^{-1}	324.97	328.30
Lattice parameters	Table 1	Table 1
Calculated density, g cm^{-3}	7.28	7.47
Absorption coefficient, mm^{-1}	32.2	33.8
F(000), e	556	560
Crystal size, μm^3	$20 \times 20 \times 30$	$20 \times 20 \times 50$
Transm. ratio (max/min)	0.41/0.29	0.57/0.27
Diffractomer	CAD4	IPDS-II
X-Ray source, Mo	sealed tube	sealed tube
Detector	PSD	Imaging Plate
Detector distance, mm	–	70
Exposure time, sec	–	1800
ω range; increment, deg	–	0 – 180; 1.0
Integr. parameter A; B; EMS	–	12.5; 2.6; 0.012
θ range, deg	2 – 35	2 – 32
Range in hkl	± 7, ± 7, ± 26	± 6, ± 6, ± 24
Total no. reflections	4802	2728
Independent reflections/R_{int}	297/0.0342	234/0.1101
Reflections with $I > 2\,\sigma(I)/R_\sigma$	223/0.0107	129/0.0475
Data/parameters	297/12	234/12
Goodness-of-fit on F^2	1.142	1.069
$R1/wR2$ for $I > 2\,\sigma(I)$	0.0135/0.0241	0.0512/0.1417
$R1/wR2$ for all data	0.0225/0.0266	0.0840/0.1558
Extinction coefficient	0.0012(2)	0.004(1)
Largest diff. peak/hole, e Å^{-3}	1.13/ – 0.70	2.69/ – 4.56

sitions were assumed again in the following cycles. The final difference Fourier syntheses revealed no residual peaks. The refined atomic positions, equivalent isotropic displacement parameters, and interatomic distances (exemplarily for PrZnSn) are given in Tables 3 and 4.

Further details of the crystal structure investigation may be obtained from Fachinformationszentrum Karlsruhe, 76344 Eggenstein-Leopoldshafen, Germany (fax: +49-7247-808-666; e-mail: crysdata@fiz-karlsruhe.de, http://www.fiz-karlsruhe.de/request_for_deposited_data.html) on quoting the deposition number CSD-426466 (PrZnSn) and CSD-426467 (NdZnSn).

Table 4. Interatomic distances (pm) of PrZnSn and PrZnSnH$_{1.5}$ (assuming the positional parameters of CeZnSnH$_{1.5}$ [22]). Standard deviations are all equal or smaller than 0.1 pm.

			PrZnSn	PrZnSnH$_{1.5}$
Pr1:	6	Sn	325.6	330.0
	6	Zn	366.2	336.4
	2	Pr2	412.6	426.9
	6	Pr1	455.4	448.0
Pr2:	6	Zn	306.6	334.2
	6	Sn	343.1	340.8
	2	Pr1	412.6	426.9
	6	Pr2	455.4	448.0
Zn:	3	Sn	270.3	258.8
	3	Pr2	306.6	334.2
	1	Zn	315.2	423.5
	3	Pr1	366.2	336.4
Sn:	3	Zn	270.3	258.8
	3	Pr1	325.6	330.0
	3	Pr2	343.1	340.8

Discussion

Crystal chemistry

PrZnSn and NdZnSn crystallize with the hexagonal YPtAs-type structure [32], space group $P6_3/mmc$, a superstructure of the aristotype AlB_2 [3]. The zinc and tin atoms form puckered $[Zn_3Sn_3]$ hexagons with a stacking sequence $AA'BB'$ along the crystallographic c axis. Previous studies [24, 25] reported only subcell data. They assumed a $CaIn_2$-type arrangement ($2c$ superstructure with respect to AlB_2) with Zn/Sn mixing. Most likely the weak superstructure reflections have not correctly been interpreted. The single-crystal data reported herein fully underline the Rietveld refinement by Manfrinetti and Pani [26] with quadrupled c axis.

In the following we briefly discuss the structural properties of PrZnSn and its hydride. The Zn–Sn dis-

Atom	Wyckoff position	x	y	z	$U_{11} = U_{22}$	U_{33}	U_{eq}
PrZnSn							
Pr1	$2a$	0	0	0	80(1)	77(1)	79(1)
Pr2	$2b$	0	0	1/4	68(1)	68(1)	68(1)
Zn	$4f$	1/3	2/3	0.15449(4)	84(2)	209(3)	126(1)
Sn	$4f$	1/3	2/3	0.61641(2)	65(1)	98(1)	76(1)
NdZnSn							
Nd1	$2a$	0	0	0	133(10)	192(10)	153(7)
Nd2	$2b$	0	0	1/4	119(10)	185(10)	141(7)
Zn	$4f$	1/3	2/3	0.1547(3)	107(14)	383(26)	199(10)
Sn	$4f$	1/3	2/3	0.6160(2)	119(8)	210(9)	149(6)

Table 3. Atomic coordinates and anisotropic displacement parameters (pm^2) of PrZnSn and NdZnSn. $U_{13} = U_{23} = 0$; $U_{12} = 1/2U_{11}$. U_{eq} is defined as one third of the trace of the orthogonalized U_{ij} tensor.

Table 5. Magnetic data for PrZnSn, NdZnSn, and their hydrides. μ_{exp} and μ_{theo}: experimental and theoretical effective magnetic moment per *RE* atom; θ_P: paramagnetic Curie temperature; T_M: magnetic ordering temperature; T_C: Curie temperature and T_N: Néel temperature.

Compound	μ_{exp} (in μ_B per *RE* atom)	θ_P (K)	T_M (K)	μ_{theo} (in μ_B per *RE* atom)
PrZnSn	3.63	−2.58(3)	$T_N = 4.7(1)$	3.58
PrZnSnH$_{1.5}$	3.25	6.0(5)	$T_C = 12.0$	3.58
NdZnSn	3.71	−9.5(5)	6.5	3.62
NdZnSnH$_{1.5}$	3.54	8.5	7.2/14.5	3.62

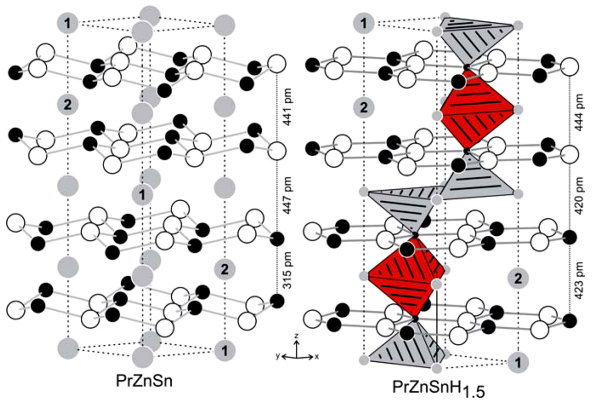

Fig. 1 (color online). The crystal structures of PrZnSn and PrZnSnH$_{1.5}$. Praseodymium, zinc and tin atoms are drawn as medium grey, black filled and open circles, respectively. The [ZnSn] networks and relevant interatomic distances are emphasized. The greyish tetrahedra are fully occupied by hydrogen, while only half of the reddish tetrahedra can be occupied for steric reasons. For details see text.

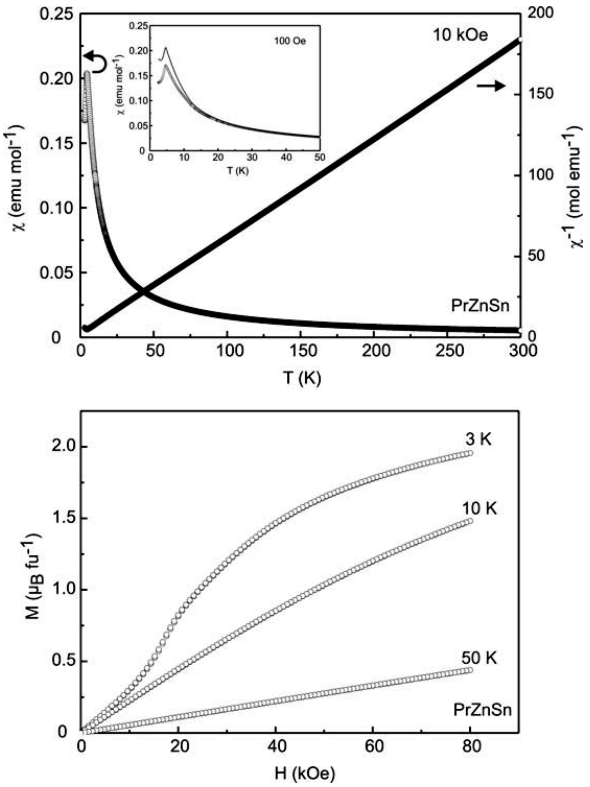

Fig. 2. Top: Temperature dependence of the magnetic susceptibility (χ and χ^{-1} data) of PrZnSn measured at 10 kOe. The low-temperature behavior (ZFC and FC data at 100 Oe) is shown in the inset. Bottom: Magnetization isotherms at 3, 10 and 50 K.

tances within the slightly puckered [Zn_3Sn_3] hexagons of PrZnSn (Fig. 1) are 270 pm (Table 4), only slightly longer than the sum of the covalent radii [33] of 265 pm. The fourth tin neighbor in the adjacent layer is at the much longer Zn–Sn distance of 447 pm. An almost ideal tetrahedral [ZnSn] network occurs in the Zintl phase EuZnSn [34] with Zn–Sn distances ranging from 278 to 305 pm.

Between the layers A and A′ as well as between B and B′, the zinc atoms point towards each other. However, the Zn–Zn distance of 315 pm (Table 4) is still significantly longer than in *hcp* zinc (6 × 266 and 6 × 291 pm Zn–Zn) [35]. This Zn–Zn distance is not indicative for Zn–Zn bonding in PrZnSn. For more details on chemical bonding in the *RE*ZnSn stannides we refer to our electronic structure calculations performed on CeZnSn [22].

Hydrogen insertion into PrZnSn and NdZnSn leads to drastic anisotropic changes in the cell parameters. Similar to CeZnSnH$_{1.5}$ [22] we observe a decrease of the *a* and an increase of the *c* lattice parameters (Table 1), and a drastic flattening of the [Zn_3Sn_3] hexagons. The course of the lattice parameters for the ternary stannides and their corresponding hydrides follows the expected lanthanide contraction. The hydrogen atoms fill two types of RE_3Zn tetrahedra (Fig. 1). For steric reasons, only half of the red-shaded tetrahedra can be filled, leading to the compositions *RE*ZnSnH$_{1.5}$. The flattening of the polyanionic

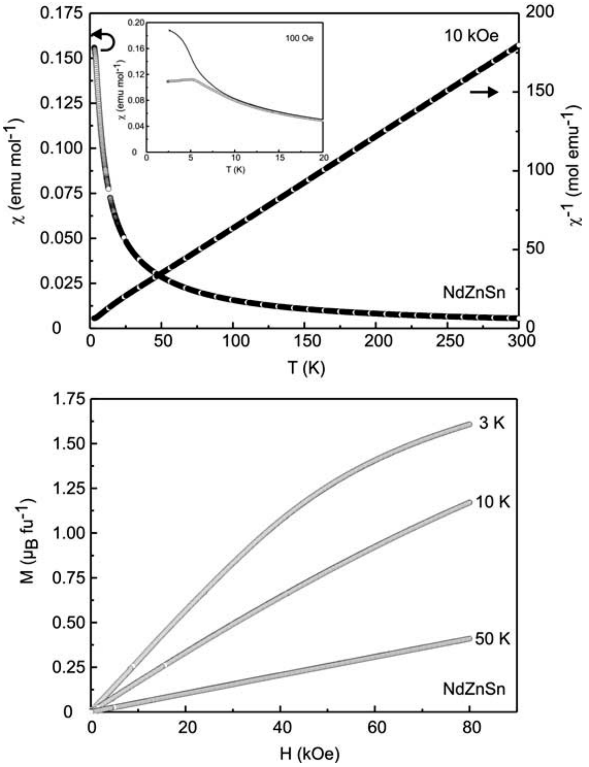

Fig. 3. Top: Temperature dependence of the magnetic susceptibility (χ and χ^{-1} data) of NdZnSn measured at 10 kOe. The low-temperature behavior (ZFC and FC data at 100 Oe) is shown in the inset. Bottom: Magnetization isotherms at 3, 10 and 50 K.

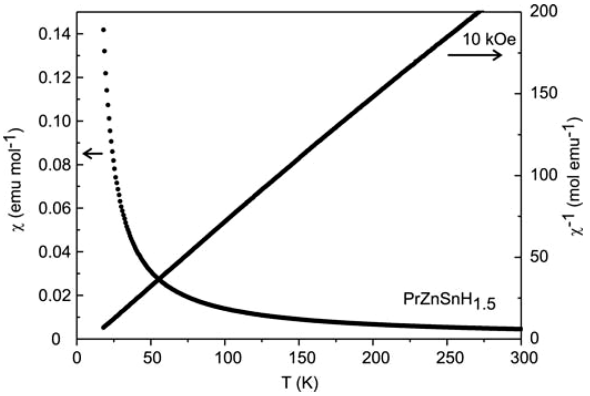

Fig. 4. Temperature dependence of the magnetic susceptibility (χ and χ^{-1} data) of $PrZnSnH_{1.5}$ measured at 10 kOe.

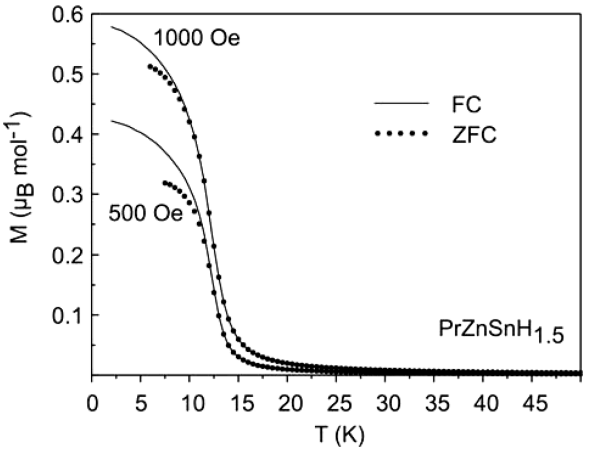

Fig. 5. The low-temperature behavior of the magnetization (ZFC and FC data at 500 and 1000 Oe) of $PrZnSnH_{1.5}$.

layers strongly influences the rare earth coordination (Table 4) and thus the magnetic ground state.

Magnetic properties

The magnetization of PrZnSn and NdZnSn has been measured between 3 and 300 K, and the results are reported in Figs. 2 and 3. Above 25 K, the magnetic susceptibility of these ternary stannides perfectly follows a Curie–Weiss behavior $\chi = C/(T + \theta_p)$ where C is the Curie constant ($C = \mu_{exp}^2/8$ with μ_{exp} the experimental effective moment per Pr or Nd atom) and θ_p is the paramagnetic Curie temperature. The μ_{exp} moments derived from the Curie constants (Table 5) are close to the theoretical values (μ_{theo}) expected for the free ions Pr^{3+} and Nd^{3+}. Moreover, the negative values of θ_p (Table 5) suggest mainly antiferromagnetic interactions for these two compounds.

The magnetization of PrZnSn has been measured at low temperatures with an applied magnetic field of 100 Oe (inset of Fig. 2; 1 kOe = 7.96×10^4 A m^{-1}); the sample was cooled in zero field (ZFC) or in a field (FC). The two curves exhibit a maximum around 4.7 K, but an irreversibility between the ZFC and FC branches appears below 12 K. At 3 K, the magnetization of PrZnSn increases linearly with the *H* field up to 12 kOe and more rapidly after the metamagnetic transition. All results suggest that PrZnSn orders antiferromagnetically below $T_N = 4.7$ K, but with a small canting of the magnetic moments explaining the presence of the irreversibility of the magnetization measured in the ZFC or FC mode. The same behavior appears for NdZnSn (Fig. 3). This compound shows a magnetic

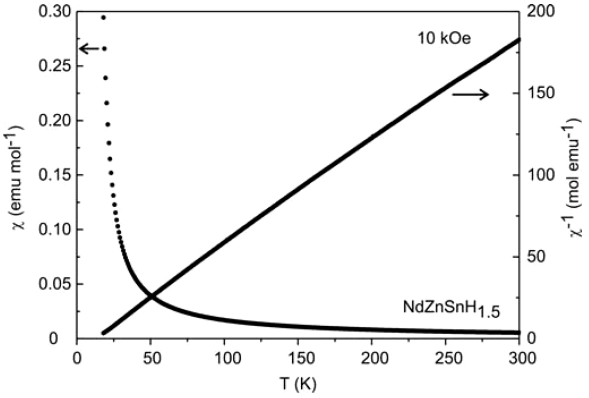

Fig. 6. Temperature dependence of the magnetic susceptibility (χ and χ^{-1} data) of NdZnSnH$_{1.5}$ measured at 10 kOe.

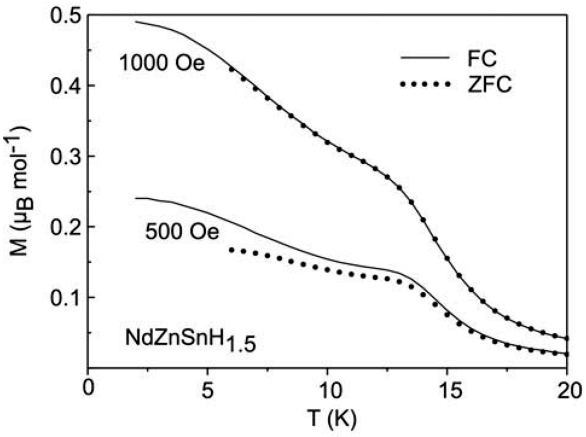

Fig. 7. The low-temperature behavior of the magnetization (ZFC and FC data at 500 and 1000 Oe) of NdZnSnH$_{1.5}$.

transition below 6.5 K, and at 3 K its magnetization increases linearly with the magnetic field up to 30 kOe and then tends to saturate. Low-temperature neutron diffraction experiments have to be performed to solve the magnetic structures of these two ternary stannides PrZnSn and NdZnSn.

Figs. 4 – 7 summarize the preliminary magnetization measurements performed on the hydrides PrZnSnH$_{1.5}$ and NdZnSnH$_{1.5}$. Fig. 5 exhibits the variation of the magnetization M of PrZnSnH$_{1.5}$ measured at low temperature in two applied magnetic fields (500 and 1000 Oe). For this hydride, the strong increase of M with decreasing T characterizes the occurrence of a ferromagnetic ordering. The Curie temperature T_C, determined from the inflection point of the $M = f(T)$ curve is 12 K. In other words, the hydrogenation of PrZnSn induces a transition from antiferromagnetic to ferromagnetic with an increase of the ordering temperature. The other hydride, NdZnSnH$_{1.5}$, shows also a ferromagnetic behavior at low temperature (Fig. 7), but for this compound two magnetic transitions are evident at 14.5 and 8.5 K.

Above 20 K, the magnetic susceptibility of these two hydrides (Figs. 4 and 6) follows a Curie-Weiss law giving positive paramagnetic Curie temperatures (Table 5) in agreement with their ferromagnetic behavior. Also, the effective magnetic moments μ_{exp} (Table 5) deduced from these measurements are comparable to those calculated for the free Pr^{3+} and Nd^{3+} ions.

Acknowledgement

We thank Dr. M. Eul for preliminary susceptibility measurements. This work was supported by the Deutsche Forschungsgemeinschaft.

[1] R. V. Skolozdra, in *Handbook on the Physics and Chemistry of Rare Earths* (Eds.: K. A. Gschneidner, Jr., L. Eyring), Vol. 24, **1997**, chapter 164, pp. 399 – 517.
[2] G. Nuspl, K. Polborn, J. Evers, G. A. Landrum, R. Hoffmann, *Inorg. Chem.* **1996**, *35*, 6922.
[3] R.-D. Hoffmann, R. Pöttgen, *Z. Kristallogr.* **2001**, *216*, 127.
[4] M. D. Bojin, R. Hoffmann, *Helv. Chim. Acta* **2003**, *86*, 1653.
[5] E. Parthé, L. Gelato, B. Chabot, M. Penzo, K. Cenzual, R. Gladyshevskii, TYPIX – Standardized Data and Crystal Chemical Characterization of Inorganic Structure Types, *Gmelin Handbook of Inorganic and Organometallic Chemistry*, 8th ed., Springer, Berlin **1993**.
[6] M. F. Zumdick, R. Pöttgen, *Z. Kristallogr.* **1999**, *214*, 90.
[7] M. F. Zumdick, R.-D. Hoffmann, R. Pöttgen, *Z. Naturforsch.* **1999**, *54b*, 45.
[8] A. E. Dwight, *Proc. Rare Earth Res. Conf., 12th*, Colorado **1976**, *1*, 480.
[9] C. Lee, M.-H. Whangbo, J. Köhler, *Z. Anorg. Allg. Chem.* **2007**, *633*, 2631.
[10] J. F. Riecken, W. Hermes, B. Chevalier, R.-D. Hoffmann, F. M. Schappacher, R. Pöttgen, *Z. Anorg. Allg. Chem.* **2007**, *633*, 1094.

[11] S. F. Matar, J. F. Riecken, B. Chevalier, R. Pöttgen, A. Al Alam, V. Eyert, *Phys. Rev. B* **2007**, *76*, 174434.
[12] A. Ślebarski, M. B. Maple, R. E. Baumbach, T. A. Sayles, *Phys. Rev. B* **2008**, *77*, 245133.
[13] J. Goraus, A. Ślebarski, *Phys. Stat. Sol. B* **2013**, *250*, 533.
[14] J. F. Riecken, G. Heymann, T. Soltner, R.-D. Hoffmann, H. Huppertz, D. Johrendt, R. Pöttgen, *Z. Naturforsch.* **2005**, *60b*, 821.
[15] G. Heymann, J. F. Riecken, S. Rayaprol, S. Christian, R. Pöttgen, H. Huppertz, *Z. Anorg. Allg. Chem.* **2007**, *633*, 77.
[16] J. F. Riecken, G. Heymann, W. Hermes, U. Ch. Rodewald, R.-D. Hoffmann, H. Huppertz, R. Pöttgen, *Z. Naturforsch.* **2008**, *63b*, 695.
[17] B. Chevalier, J.-L. Bobet, M. Pasturel, E. Bauer, F. Weill, R. Decourt, J. Etourneau, *Chem. Mater.* **2003**, *15*, 2181.
[18] F. Weill, M. Pasturel, J.-L. Bobet, B. Chevalier, *J. Phys. Chem. Solids* **2006**, *67*, 1111.
[19] B. Chevalier, C. P. Sebastian, R. Pöttgen, *Solid State Sci.* **2006**, *8*, 1000.
[20] B. Chevalier, A. Wattiaux, J.-L. Bobet, *J. Phys.: Condens. Matter* **2006**, *18*, 1743.
[21] A. Aburto, E. Orgaz, *Phys. Rev. B* **2007**, *75*, 045130.
[22] W. Hermes, B. Chevalier, U. Ch. Rodewald, S. F. Matar, F. Weill, I. Schellenberg, R. Pöttgen, H. Lueken, M. Speldrich, *Chem. Mater.* **2011**, *23*, 1096.
[23] W. Hermes, S. F. Matar, T. Harmening, U. Ch. Rodewald, M. Eul, R. Pöttgen, *Z. Naturforsch.* **2009**, *64b*, 175.
[24] P. S. Salamakha, P. Y. Demchenko, O. L. Sologub, O. I. Bodak, *Pol. J. Chem.* **1999**, *73*, 885.
[25] P. Demchenko, O. I. Bodak, *J. Alloys Compd.* **2000**, *307*, 215.
[26] P. Manfrinetti, M. Pani, *J. Alloys Compd.* **2005**, *393*, 180.
[27] R. Pöttgen, Th. Gulden, A. Simon, *GIT Labor-Fachzeitschrift* **1999**, *43*, 133.
[28] R. Pöttgen, A. Lang, R.-D. Hoffmann, B. Künnen, G. Kotzyba, R. Müllmann, B. D. Mosel, C. Rosenhahn, *Z. Kristallogr.* **1999**, *214*, 143.
[29] K. Yvon, W. Jeitschko, E. Parthé, *J. Appl. Crystallogr.* **1977**, *10*, 73.
[30] G. M. Sheldrick, SHELXL-97, Program for the Refinement of Crystal Structures, University of Göttingen, Göttingen (Germany) **1997**.
[31] G. M. Sheldrick, *Acta Crystallogr.* **2008**, *A64*, 112.
[32] G. Wenski, A. Mewis, *Z. Kristallogr.* **1986**, *176*, 125.
[33] J. Emsley, *The Elements*, Oxford University Press, Oxford **1999**.
[34] R. Pöttgen, *Z. Kristallogr.* **1996**, *211*, 884.
[35] J. Donohue, *The Structures of the Elements*, Wiley, New York **1974**.